



**HAL**  
open science

## Characterizing Nanoparticle Mass Distributions Using Charge-Independent Nanoresonator Mass Spectrometry

Szu-Hsueh Lai, Adrien Reynaud, Ning-Ning Zhang, Minjeong Kwak, Bogdan Vysotskyi, Sergio Dominguez-Medina, Thomas Fortin, Kavya Clement, Martial Defoort, Tae Geol Lee, et al.

### ► To cite this version:

Szu-Hsueh Lai, Adrien Reynaud, Ning-Ning Zhang, Minjeong Kwak, Bogdan Vysotskyi, et al.. Characterizing Nanoparticle Mass Distributions Using Charge-Independent Nanoresonator Mass Spectrometry. *Journal of Physical Chemistry C*, 2022, 126 (49), pp.20946-20953. 10.1021/acs.jpcc.2c06675 . hal-04019924

**HAL Id: hal-04019924**

**<https://hal.science/hal-04019924>**

Submitted on 26 Oct 2023

**HAL** is a multi-disciplinary open access archive for the deposit and dissemination of scientific research documents, whether they are published or not. The documents may come from teaching and research institutions in France or abroad, or from public or private research centers.

L'archive ouverte pluridisciplinaire **HAL**, est destinée au dépôt et à la diffusion de documents scientifiques de niveau recherche, publiés ou non, émanant des établissements d'enseignement et de recherche français ou étrangers, des laboratoires publics ou privés.



Distributed under a Creative Commons Attribution - NonCommercial 4.0 International License

# Characterizing Nanoparticle Mass Distributions Using Charge-Independent Nanoresonator Mass Spectrometry

Szu-Hsueh Lai<sup>1,4,5</sup>, Adrien Reynaud<sup>2,4</sup>, Ning-Ning Zhang<sup>6</sup>, Min Jeong Kwak<sup>7</sup>, Bogdan Vysotskyi<sup>2,4‡</sup>, Sergio Dominguez-Medina<sup>1,3,4,◇</sup>, Thomas Fortin<sup>1</sup>, Kavya Clement<sup>1,3,4</sup>, Martial Defoort<sup>2,4†</sup>, Tae Geol Lee<sup>7#</sup>, Kun Liu<sup>6#</sup>, Sébastien Hentz<sup>2,4#</sup>, Christophe D. Masselon<sup>1,3,4\*</sup>

<sup>1</sup>CEA, IRIG, Biologie à Grande Echelle, F-38054 Grenoble, France

<sup>2</sup>CEA, LETI, MINATEC Campus, F-38054 Grenoble, France

<sup>3</sup>Inserm, Unité 1092, F-38054 Grenoble, France

<sup>4</sup>Université Grenoble Alpes, F-38000 Grenoble, France

<sup>5</sup>Department of Chemistry, National Cheng Kung University, Tainan 701, Taiwan

<sup>6</sup>State Key Laboratory of Supramolecular Structure and Materials, College of Chemistry, Jilin University, Changchun 130012, China

<sup>7</sup>Korea Research Institute of Standards and Science (KRISS), Yuseong-Gu, South-Korea

\* Corresponding author: christophe.masselon@cea.fr

# Senior author

† Current address: Université Grenoble Alpes, CNRS, Grenoble INP, TIMA, 38000 Grenoble, France

‡ Current address: IMEC, Kapeldreef 75, 3001 Leuven, Belgium

◇ Current address: Folio Photonics Inc., 6864 Cochran Rd, Solon, OH 44139

### *Abstract (250 words)*

Due to their unique size-dependent properties, nanoparticles (NPs) have many industrial and biomedical applications. Although NP are generally characterized based on size or morphological analysis, the mass of whole particles can be of interest as it represents the total amount of material in the particle regardless of shape, density, or elemental composition. In addition, the shape of non-spherical NPs presents a conceptual difficulty making them difficult to characterize in terms of size or morphological characteristics. Here, we used a novel nano-electro-mechanical sensor mass spectrometry (NEMS-MS) technology to characterize the mass distributions of various NPs. For standard spherical gold NPs, mass distributions covered the range from ~5 to 250 MDa (8 to ~415 attograms). Applying the density of gold (19.3 g/cm<sup>3</sup>) and assuming perfect sphericity, these mass measurements were used to compute equivalent diameters of the NPs. The sizes determined agreed well with transmission electron microscope (TEM) imaging data, with deviations of ~1.4%. Subsequently, we analyzed the mass distribution of ~50-nm synthetic silicon dioxide particles, having determined their size by electron microscopy (SEM and TEM). Their estimated density was in line with literature values derived from differential mobility analyzer (DMA) and aerosol particle mass analyzer (APM) data. Finally, we examined intact gold nanotetrapods (NTPs) and obtained a mass distribution revealing their controlled polydispersity. The presence of polyethylene glycol (PEG) coating was also quantified and corroborated nuclear magnetic resonance (NMR) observations. Our results demonstrate the potential of NEMS-MS-based measurements as an effective means to characterize nanoparticles, whatever their shape or density.

### *Keywords*

Nanoelectromechanical sensor, Mass spectrometry, Nanoparticle, Single-particle characterization, Intact mass.

### *Abbreviations*

NP: Nanoparticle; NEMS: Nano-Electro-Mechanical Sensor; MS: Mass Spectrometry; TEM: Transmission Electron; SEM: Transmission Electron Microscopy; DMA: Differential Mobility Analyzer; NTP: (Gold) Nanotetrapods; PEG: Polyethylene Glycol; NMR: Nuclear Magnetic Resonance; DLS: Dynamic Light Scattering; NTA: Nanoparticle Tracking Analysis; SAXS: Small Angle X-Ray Scattering; AFM: Atomic Force Microscopy; PMD: Particle Mass Distribution; ICP: Inductively Coupled Plasma; PSD: Particle Size Distribution; GPC: gel permeation chromatography

Thanks to their tunable physical, chemical, and biological properties, nanoparticles (NPs) have attracted tremendous interest in industrial as well as biomedical applications.<sup>1</sup> As an example, synthetic gold NPs have been widely used in industry and academia in sensing,<sup>2</sup> electron microscopy,<sup>3</sup> materials science,<sup>4</sup> and biomedical research applications.<sup>5</sup> Likewise, non-metallic particles such as silica NPs have widespread applications in polishing and as additives to drugs, cosmetics, printer toners, and foodstuffs.<sup>6,7</sup> The rapid increase in production of synthetic NPs has been accompanied by inevitable issues related to concerns surrounding environmental contamination and human toxicity.<sup>1,8</sup> Therefore, it is particularly important that appropriate scientific tools be developed to characterize both synthetic and natural NPs.

As nanomaterials exhibit size-dependent properties that determine their physical characteristics and how they interact with their environment, size is considered the critical parameter directly related to their practical applications.<sup>9</sup> Therefore, several technologies have been used to characterize NPs, including light scattering approaches (*e.g.*, DLS, nanoparticle tracking analysis, small-angle x-ray scattering)<sup>10</sup> and imaging technologies (*e.g.*, atomic force microscopy, SEM, TEM)<sup>11</sup> as a means to estimate size or glean morphological details. In practice, the average size of an NP sample is obtained by measuring either a group of particles (*i.e.*, ensemble measurement), or a large number of individual particles and determining a distribution (*i.e.*, single-particle measurement). Thus, particle size is always represented by a distribution of values, which can be fitted to a probability distribution providing an average particle size and its associated uncertainty, combining instrumental error and the intrinsic size distribution of the sample. Unfortunately, most of the methods used to characterize NPs have specific limitations due to limited descriptors (1D- or 2D-rendition of 3D particles), or to an inability to characterize particles that are either non-spherical or of heterogeneous composition. Consequently, different methods applied to the same sample often provide discordant size descriptions. For instance, characterization of NIST 10-nm gold nanoparticles yielded sizes ranging from  $8.5 \pm 0.3$  nm to  $11.3 \pm 0.1$  nm depending on the method used.<sup>12</sup> These discrepancies may result from various biases in size estimations due to lateral resolution, and/or from invalid sphericity assumptions.

In an attempt to overcome these difficulties, particle mass distribution (PMD) can be used in complement to other NP characterization methods. Mass is a fundamental parameter that is used to identify and classify molecules as well as particles. Unlike size determination, mass measurements explicitly account for the three-dimensional nature of NPs and their associated density, even when these characteristics are not uniform across the whole particle, such as in the case of hollow or composite nanoparticles.<sup>13</sup>

Mass spectrometry (MS) is a powerful tool used in many fields to weigh molecules and characterize their structures through fragmentation. In 2016, Zhang *et al.*<sup>14</sup> reported mass measurements of individual NPs using a specially designed ion-quadrupole-ion trap combined with particle detection by light scattering microscopy. In their setup, particles were irradiated by a UV lamp to induce charge variation through photoelectric effects, and the mass-to-charge ratio ( $m/z$ ) and the number of elementary charges ( $z$ ) carried by individual NPs were repeatedly determined. Although promising, the method suffered from inadequate statistics as each particle was monitored multiple times, and from a complex mass determination scheme based on the Mathieu equation. In addition, the authors reported extensive aggregation issues. To measure the mass of intact macromolecular ions, the leading technology is charge detection mass spectrometry (CDMS).<sup>15</sup> Like Zhang *et al.*<sup>14</sup>, CDMS also measures  $m/z$  and  $z$  for individual particles in order to

derive their mass. However, for NP analysis – especially for particles that ionize poorly – the reliance of CDMS on ionization limits its applicability. Alternatively, commercially available inductively coupled plasma mass spectrometry (ICP-MS) operated in single-particle mode can be used to determine the elemental composition of NPs by quantifying specific atomic ions.<sup>16</sup> Analytes are ionized in plasma and dissociated into elementary ions, which are sorted based on their atomic masses. Therefore, the weight of individual particles can be determined following appropriate quantitative calibration of ion intensities, and particle size derived if the corresponding density is known. Nevertheless, several types of NP are not amenable to ICP-MS due to its intrinsic low sensitivity for some elementary ions (*e.g.*, C, Si). Hence, ICP-MS analysis of silica NP, as well as organic or polymer-coated inorganic NPs present intractable challenges.

A new type of mass spectrometry technology based on nano-electromechanical sensors (NEMS) is emerging that allows charge-independent mass analysis in the mega- to giga-Dalton (~attogram to femtogram) range.<sup>17</sup> This technology has specific advantages over ICP-MS and CDMS, such as its ability to characterize the inertial mass of intact individual particles, regardless of their elemental composition or ionization efficiency. In the study presented here, we investigated the usefulness of NEMS-based mass spectrometry for NP characterization. For this purpose, we analyzed various NP standards, such as synthetic sphere-like gold NPs and silica NPs with characteristic sizes ranging from ~15 to 50 nm in diameter. Furthermore, we measured the PMD of non-spherical gold nanotetrapods (NTPs), which are impossible to adequately describe using a single-dimensional parameter. Our results demonstrate the potential of inertial mass measurement of intact NPs using NEMS-MS as a complement to size and morphological characterization.

## Results and Discussion

Particle size distribution (PSD) is one of the key factors revealing the relationship between NP size and physical properties.<sup>18</sup> Currently, it is also the major parameter used to evaluate the polydispersity of NPs. However, using a 1D descriptor such as the diameter to represent 3D structures, especially for non-spherical and irregularly shaped particles, can present intractable challenges. An alternative complementary strategy is to measure the PMD. Nanomechanical mass sensors have been used in the past to characterize individual NPs<sup>19</sup>, but the capacity to directly derive NP inertial mass distributions using NEMS-based MS has only recently become available.<sup>17</sup>

### Benchmarking NEMS mass measurements with sphere-like gold NPs

To benchmark the performance of NEMS-MS for PMD determination, we first analyzed commercial 15-nm and 30-nm sphere-like gold NPs with masses anticipated to lie in the 15-20 MDa and 100-250 MDa ranges, respectively. Results were plotted and are summarized in **Figure 1** and **Table 1**, **Error! Reference source not found.** respectively.

The inset in **Figure 1a** shows the mass distribution for 15-nm gold NPs based on a series of measurements made under the same operating conditions, repeated on multiple non-consecutive or consecutive days over a week. Importantly, the measurement on the last day was performed after changing the nanoresonator array. The number of particles detected in these measurements ranged from ~400 to 1300 depending on the total duration of the experiment. As illustrated by the box and violin plots, only minor differences were found across days and arrays. Slight day-to-day variations could be attributed to uncontrolled variations in sampling, aggregation, ESI conditions, or partially incomplete desolvation. When these four populations were fitted to a Gaussian distribution model using non-linear least-squares fitting, variations in the average and

standard deviation did not exceed 1.3 MDa and 0.5 MDa, respectively. Notably, taking these measurements into account, the standard uncertainty for the 15-nm gold PMD ( $\sim 0.3$  MDa) corresponded to a  $\pm 0.08$ -nm deviation in diameter for perfectly spherical particles (see **Figure 1b**). This level of measurement uncertainty compares favorably with current size-characterization technologies such as TEM.<sup>11</sup> However, it should be noted that the uncertainty with NEMS measurements is density-dependent, and in this particular case is very low due to the high density of gold. The limit of detection (LOD) of our NEMS devices, which was previously estimated from the resonator's quality factor and frequency noise level, is approximately 0.5 MDa.<sup>20</sup> The mass uncertainty over multiple measurements was close to the LOD. These results indicate the stability and consistency of NEMS-MS measurements over several days or when using distinct arrays.

A spectrum consisting of 3,437 mass detection events was obtained by combining the four datasets from 15-nm gold NP measurements. This combined spectrum improved precision due to its greater number of points, and thus more robust statistics. The overall mean mass was 18.0 MDa with a standard deviation of 5.7 MDa (**Figure 1a**). Incidentally, this happens to be the smallest mass standard reported using our current NEMS-MS system design. Using the density of gold ( $19.3 \text{ g/cm}^3$ ) and applying the spherical particle hypothesis, a mean diameter of 14.4 nm was calculated. This value was in excellent agreement with the average size reported from TEM images (14.2 nm).

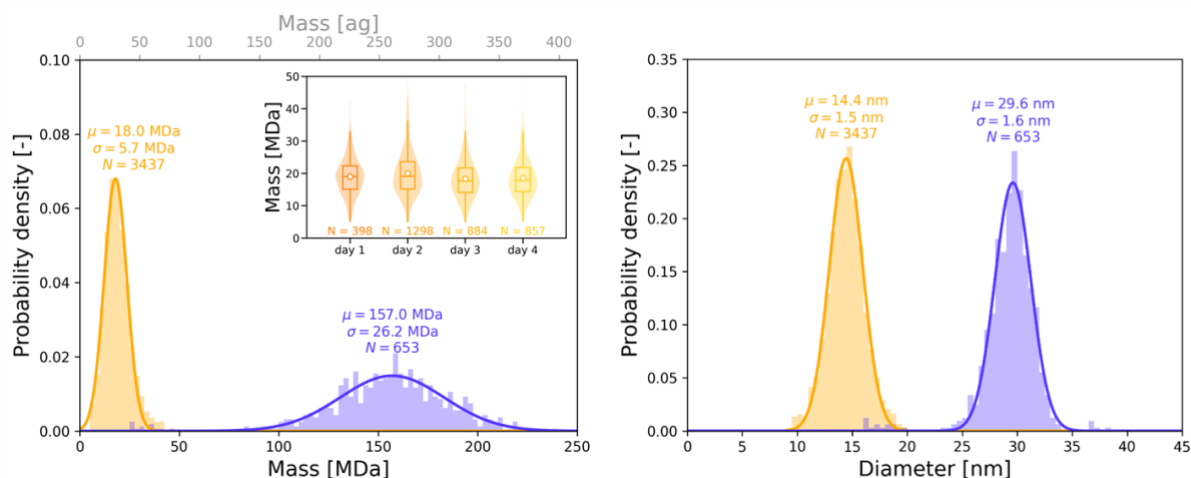


**Figure 1** – Overlaid mass distributions for two commercial gold nanoparticle samples (a) and overlaid size distributions derived from the mass distributions, assuming uniform density and perfectly spherical shape (b). The inset in (a) shows the results from repeated measurements of the 15-nm gold NP sample on multiple consecutive and non-consecutive days over a week, with two distinct nanoresonator arrays.

We performed similar analyses on 30-nm sphere-like gold NPs to assess the upper mass range ( $> 150$  MDa). For these NPs, 653 individual particles were recorded, the mass determined, 157.0 MDa, corresponded to a computed average diameter of 29.6 nm based on the density of gold and the hypothesis that the particles are perfectly spherical (**Figure 1b**). In line with the results for the 15-nm NP, the average size of the 30-nm gold NPs computed from mass measurements was about 1.4% larger than the TEM-based size indicated by the supplier. All these measurements of sphere-like gold NP standards substantiate the suitability of NEMS-MS for the characterization of intact NPs using mass measurement.

**Table 1** – NEMS-MS-derived diameter and mass compared to supplier’s specifications.

Supplier specifications (TEM)		NEMS-MS		Relative differences	
Measured mean diameter $\pm$ S.D.	Computed mean mass*	Computed mean diameter $\pm$ S.D.	Measured mean mass	Diameter	Mass
(nm)	(MDa)	(nm)	(MDa)	%	%
14.2 $\pm$ 0.9	17.4	14.4 $\pm$ 1.5	18.0	1.4	2.9
29.2 $\pm$ 2.1	151.7	29.6 $\pm$ 1.6	157.0	1.4	3.5

\* Using the density of gold (19.3 g·cm<sup>-3</sup>) and assuming perfect sphericity.

## Density characterization of amorphous silica nanoparticles

Korea Research Institute of Standards and Science (KRISS) manufactured a series of size-controlled spherical silica nanoparticles (diameter ranging from 20 to 90 nm) displaying narrow size distributions (standard deviation < 3.2 nm).<sup>21</sup> These particles have been thoroughly characterized using a broad variety of methodologies, and constitute a suitable alternative to polystyrene nanospheres as standards for instrument calibration. Although the size of these particles could be readily determined using (*e.g.*) electron microscopy, other physical properties such as density and weight are more challenging to access, and application of several methods produced non-convergent estimates (Certificated Reference Material: 301-04-001).

Here, we investigated the density of ~50 nm SiO<sub>2</sub> NPs using electron microscopy and NEMS-MS technology to measure size and mass, respectively. Size measurements according to TEM (FEI Tecnai F-30) and SEM (FE-SEM; HITACHI S-4800) analysis yielded diameters of 51.9  $\pm$  1.2 nm and 53.8  $\pm$  0.8 nm, respectively. The distribution of mass measurements acquired by NEMS-MS could be fitted by a Gaussian peak (**Figure 2a**). The resulting mean mass and standard uncertainty were 87.9  $\pm$  0.7 MDa (**Table S2.1**) and the standard deviation of the PMD was 11.1 MDa. From these assessments, we computed average densities of 1.79 and 1.99 g/cm<sup>3</sup>, depending on the method used to determine size (**Figure 2b**).

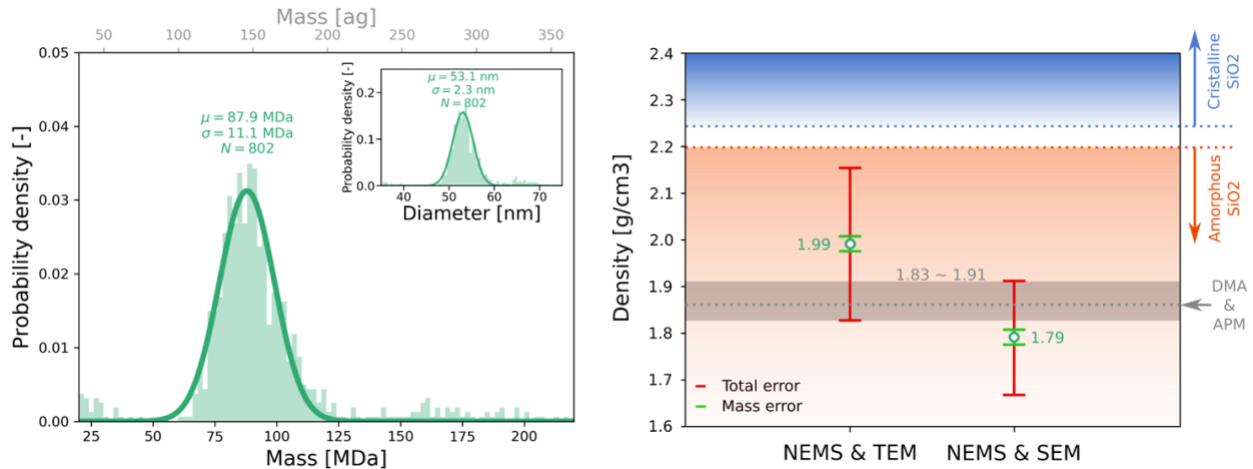


**Figure 2** – NEMS-MS derived mass distribution of ~50 nm silicon dioxide nanoparticles and inset showing the derived size distribution assuming a density of 1.9 g/cm<sup>3</sup> (a). Comparison of average density values and standard errors derived from NEMS-MS mass and electron microscopy (TEM or SEM) size measurements (b). (N: number of acquired events,  $\mu$ : location,  $\sigma$ : standard deviation of Gaussian fit)

SiO<sub>2</sub> exists in a large variety of crystalline forms with density values ranging from ~ 2.27 to 2.65 g/cm<sup>3</sup> (Handbook of Chemistry and Physics Ed 102 Online). Considering the uncertainties associated with the size and mass estimations, the density of the NPs analyzed here could be as high as 2.16 g/cm<sup>3</sup> (based on size measured by TEM), which is still lower than that of the least dense crystalline SiO<sub>2</sub> forms. As shown in **Figure 2b**, the contribution of mass uncertainty to density estimates was minor compared to the contribution of size uncertainties (**Table S2.2 and Table S2.3**). It has been reported that silica NPs appear ~3% smaller in TEM than in SEM due to their poor edge contrast.<sup>22</sup> Our observations appear consistent with these reports. This supports the range determined from SEM measurements (1.79 ±0.12 g/cm<sup>3</sup>). Although TEM and SEM results tended to diverge, there was a narrow size range (53.0-53.1 nm) over which estimates from the two methods overlapped. Based on these results, the density of silica NPs is certainly lower than that of SiO<sub>2</sub> crystalline forms, and is most likely in the range of 1.83 to 1.91 g/cm<sup>3</sup>. Interestingly, a low average density of ~1.87 g/cm<sup>3</sup> was previously reported based on differential mobility analyzer (DMA) and aerosol particle mass analyzer (APM) measurements of silica NP size standards (40-200 nm) synthesized by a sol-gel process.<sup>23</sup> Our results were in very good agreement with this density, which provides further evidence that silica NPs produced by sol-gel processes have an amorphous nature, with a corresponding lower density than crystalline forms – according to the Handbook of Chemistry and Physics (Ed 102 Online), the density of amorphous silica is in a range between 1.9 and 2.2 g/cm<sup>3</sup>. These results illustrate the relevance of NEMS-MS mass measurements to derive important properties of NPs that cannot be determined by ICP-MS (as is the case for silica NP).

### Mass characterization of non-spherical gold nanotetrapods

Nanobranched gold particles have drawn great interest for various biological and biomedical applications due to their excellent NIR plasmon resonance properties.<sup>24</sup> For instance, monodisperse gold nanotetrapods (NTPs) with tunable and ultra-narrow plasmonic bands were produced using a facile seed-mediated growth method. Upon laser irradiation, these PEGylated NTPs possess remarkable photothermal conversion efficiencies and photoacoustic imaging properties.<sup>25</sup> Although transmission electron microscopy (TEM) can be used to monitor the size and shape of synthesized NTPs, it has been difficult to identify appropriate statistical descriptors to characterize the heterogeneity of these non-spherical particles. In addition, it is not currently feasible to quantify the grafting of polymer chains (*e.g.*, PEG) onto individual NTP through size estimations. In this context, a method to determine the inertial mass of PEGylated NTPs seems particularly appealing.

As shown above, NEMS-MS technology demonstrated its ability to analyze monodisperse sphere-like NPs, however, polydisperse particles or NPs with a non-unitary aspect ratio constitute distinct challenges. To investigate this aspect, we determined the PMD for monodisperse single-crystalline gold NTPs with unique topological structures (**Figure 3a**). A growth mechanism based on kinetically-controlled deposition and diffusion of adatoms was used to produce gold NTPs with ~85% purity.<sup>25</sup> PEGylation of NTPs has been shown to significantly improve their thermal and colloidal stability, consequently, the NTPs analyzed here were PEGylated by addition of monomethoxy-poly(ethylene glycol)-thiol (mPEG-SH).

Based on TEM imaging results, a non-negligible proportion (up to 13%) of the particles produced appeared to be potentially defective (*e.g.*, irregularly shaped, missing arms), or to be pseudo-spherical (**Figure 3b**). Unfortunately, these minor species remain challenging to characterize and quantify because of the difficulty in using 2D morphology to assess underlying 3D structures. For

instance, a 3-armed structure could appear 2-armed in the image if the third arm lies perpendicular to the imaging plane. Likewise, a *bona fide* tetrapod could be mistaken for a 3-armed structure because of a hidden arm.

Faced with these uncertainties, measurement of the mass of intact NPs is complementary to imaging, in that it reveals the true polydispersity of the samples. **Figure 3c** shows the PMD of PEGylated gold NTPs using NEMS-MS technology, with a Gaussian fit over its major mode. An asymmetric distribution extending over the mass range 40-68 MDa was observed, featuring a minor mode at about 44 MDa and a major mode at ~57 MDa. Interestingly, the right side of the PMD displayed an abrupt edge, whereas the aspect on the left side was more irregular, indicating the presence of incomplete structures. In addition, low-abundance signals in the ranges 20-40 MDa and 100-130 MDa were most likely the result of damaged NPs and multimers, respectively.

The average volume of a gold NTP can be computed based on the size of its core particle, and the number, length, and width of its arms (See **Figure S3**). TEM analysis revealed that fully formed NTPs had an average arm length of  $22.2 \pm 0.6$  nm and width of  $8.0 \pm 0.5$  nm (**Figure 3a**). Furthermore, nuclear magnetic resonance (NMR) measurements using a grafting density analysis approach (**Figure S4** and **Table S4**) revealed an average of  $\sim 1954 \pm 25$  PEG chains on each gold NTP.<sup>26</sup> Based on its average molecular weight (5000 g/mol), the total mass of PEG on a gold NTP is thus  $9.8 \pm 0.2$  MDa. As a result, the intact mass of a PEGylated gold NTP could be anticipated to lie between 54 and 60 MDa.

Taking into account all these considerations, we computed the theoretical volume, mass, and fractional amounts for a variety of apparent particle shapes, yielding mass estimates in the range 44.3 to 49.8 MDa. (See **Table 2** and **Supporting Information S3**). The mass computed for the gold content of integral NTPs was close to the mass ( $48.5 \pm 1.0$  MDa) determined from ICP-MS measurement (iCAP Q, Thermo Scientific) of the number of gold atoms in individual particles (**Table S5**).

We also confirmed the thermal stability of PEG chains on a gold NTP by thermogravimetric analysis. Unlike citrate-capping ligands, thiol-terminated PEG chains form strong covalent S-Au bonds that are stable up to 250 °C.<sup>26</sup> In this study, the heated capillary temperature was set to 200 °C to allow desolvation of nebulized particles from the NTP solution. Thus, we expected NEMS-MS to measure an intact mass for NTP surrounded by PEG chains.

The results held out this expectation as the dominant peak at ~57 MDa agreed well with the intact mass of the NTP structure – as determined by ICP-MS – incremented by the number of PEG side-chains. Moreover, an estimate of the proportion of integral gold NTPs from NEMS-MS measurements was about 88% (taking into account the particle mean mass  $\pm 2$  standard deviations). This proportion is close to the relative fraction derived from TEM observations. It is also interesting to note that the calculations of the dominant side product masses converged to a value ranging from 43 to 48 MDa. Although it remains difficult to distinguish between 3-armed, 1-armed, or immature irregularly shaped particles, the coincidence in mass suggests a kinetically-controlled pathway in which mass growth continues regardless of shape. Considering the possible volume bias of the particle due to the TEM analysis and the mass deviations of the number of PEG chains on each NP, a precision within 2 MDa (~3%) between predicted mass, ICP-MS result, and NEMS-MS can be considered quite comparable. In summary, NEMS-MS technology not only

characterized the PMD of non-spherical gold NTP with PEG side-chains, but also reflected the presence of side products, which is still a challenge when using other technologies.

Table 2– Mass estimation of integral gold NTP and possible side products. – Computed particle volume, mass, and proportions for a variety of apparent particle shapes.

Shape	Integral NTPs	2 or 3 arms		1-arm (big head)	Sphere (15.1 nm diameter)	Immature (irregular)
		3 arms	2 arms			
Volume (nm <sup>3</sup> )	3804 – 4283	2985 – 3464	2166 – 2645	3392	1803	3349
Surface area (nm <sup>2</sup> )	2101	~1737	~1265	~1536	716	~1072
Mass gold atoms (MDa)	44.3 – 49.8*	34.8 – 40.3	25.3 – 30.8	39.5	21.0	39.0
Mass PEG chains (MDa)	9.8	8.1	5.9	6.7	3.3	5.0
Mass whole particle (MDa)	54.1-59.6	42.9 – 48.4	31.2 – 36.7	46.2	24.3	44.0
Relative fraction (%)#	87.1	4.7		2.0	1.6	4.7

\*48.5 MDa according to ICP-MS measurements

#Based on TEM result for 255 particles (human evaluation)

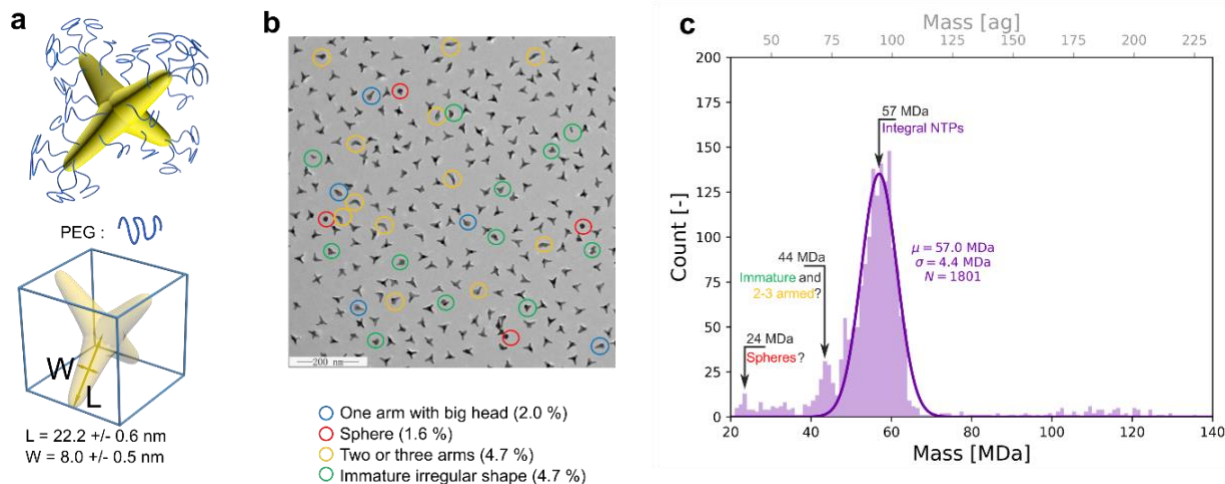


Figure 3 (a) Three-dimensional representation of a gold nanotetrapod (yellow) surrounded by PEG chains (blue fibers). (b) TEM image of gold nanotetrapods. Scale bar: 200 nm. (c) PMD of gold nanotetrapods according to NEMS-MS measurements. Data were binned to 1 MDa when plotting the mass distribution histogram which was fitted with a Gaussian distribution curve.

## Conclusion

The aim of this study was to determine the capacity of NEMS-MS to characterize NPs, whatever their shape and size. The characterization of sphere-like gold NPs of two different diameters (15 nm and 30 nm) using NEMS-MS technology returned particle masses ranging between 5 MDa and 250 MDa. Measurements of 15-nm gold NPs across experiments performed on different days and with distinct NEMS arrays showed good consistency. Based on the spherical shape hypothesis and the isotropic density of gold, the NP size computed from the NEMS-MS result deviated by a maximum of 1.4% from the value provided by the manufacturer. The density of silica NPs was also

characterized by combining size investigations (from SEM and TEM images) and NEMS-MS mass measurements. The average density determined from these measurements was about 1.9 g/cm<sup>3</sup>, which is similar to the value reported previously based on DMA and APM analyses. Finally, the PMD determined for non-spherical gold nanotetrapods (NTPs) not only confirmed the approximate number of PEG chains coating particles (as estimated by NMR) but also revealed the polydispersity of these particles. Both of these figures of merit are difficult to efficiently and precisely evaluate based on size descriptors alone. In summary, this first assessment of the NEMS-MS technology demonstrated that it is suitable for characterizing NPs nebulized from a condensed phase to the gas phase via the process of electrospray ionization (ESI). This novel addition to the nano-characterization toolbox can be applied in a straightforward manner to determine the PMD of non-spherical or heterogeneous NPs, including soot particles, or hybrid NPs.

## Material and methods

### Material and sample preparation

Gold nanoparticles measuring 15 and 30 nm in diameter (EM.GC20) suspended in citrate buffer were purchased from BBI Solutions (Crumlin, United Kingdom). They were diluted in 50% deionized water/methanol (Sigma Aldrich, Saint-Louis, Missouri, USA) to a final concentration of  $7 \times 10^{11}$  and  $1 \times 10^{11}$  particles/mL, respectively, before performing mass measurements. Amorphous silica nanoparticles (ASiNPs) measuring about 50 nm diameter were provided by the Korea Research Institute of Standards and Science (KRISS)<sup>21</sup>. They were implemented using methods modified from the protocols proposed by Hartlen *et al.*<sup>27</sup> The solution was first passed through a 0.22-micron syringe filter and then diluted 100-fold with double-distilled water to a final concentration of about  $5 \times 10^{11}$  particles/mL. Gold nanotetrapods (NTPs) were synthesized according to the method reported previously.<sup>25</sup> Freshly prepared gold NTPs were centrifuged and re-dispersed in an aqueous mPEG-SH (JenKem Technology Ltd.) solution (0.10 mg/mL). The average *M<sub>w</sub>* of mPEG-SH was 5000 g/mol, with a polydispersity of less than 1.02 as determined by gel permeation chromatography (GPC). After ligand exchange, free PEG was removed by centrifugation, and the sample was lyophilized to remove water. Lyophilized mPEG-NTPs were resuspended in 50% water-ethanol to a final concentration of about  $5 \times 10^{11}$  particles/mL before performing mass measurements.

### NEMS-MS architecture

A schematic diagram of the NEMS-MS system is shown in **Figure S6**. It is composed of three successive stages: first, a nanoelectrospray ionization (nanoESI) source is used to generate airborne particles from a colloidal solution. The liquid sample flows through a 30- $\mu$ m i.d. fused silica tip emitter (FS360-50-30-N-20-C12, PicoTip<sup>TM</sup>), and then a 2290E-5 Tektronix HV power supply (Tektronix Inc., Beaverton, United-States) nebulizes the flow by applying high voltages (2-4 kV).

Nebulized droplets containing particles then pass through a heated capillary (175-200 °C) where desolvation occurs. The particle beam is subsequently focused through an aerodynamic lens onto an array of nanomechanical sensors. The aerodynamic lens is composed of a pressure-limiting orifice followed by a series of specifically calibrated apertures and expansion chambers. The lens is designed to take advantage of a trade-off between particle inertia and Brownian diffusion. The specifications include geometric parameters (spacers between orifices, orifice diameters) and the inlet and outlet pressures (**Figure S7**). The parameters for our architecture were optimized for 100-nm diameter particles with close to unit density, in line with the guidelines presented by Wang

*et al.*<sup>28</sup>. As reported in a previous communication, the focusing system produces a ~1.5-mm cross-section beam at the chip position.

## Nano-resonators and mass calculation

The crux of the NEMS-MS architecture is the sensitive element used to measure the mass of incoming nanoparticles. In the current implementation, an electrostatically-actuated nanoresonator detects mass addition events in real-time. Thus, when a single particle lands on a nanoresonator's beam at a time  $t$ , the added mass causes the resonance frequency  $f_n$  to shift down by  $\Delta f_n$ . The relative resonance frequency shift  $\Delta f_n/f_n$  depends both on the added  $\Delta m$  and on the landing position  $x$ , as expressed in the following equation:

$$\Delta m = 2M \frac{\Delta f_n}{f_n} \frac{\alpha_n}{\phi_n^2(x)}$$

Where  $M$  is the mass of the resonator beam, the function  $\phi_n(x)$  is the mode shape of the  $n$ -th mode, and  $\alpha_n$  is a constant  $\alpha_n = -2 \int_{x=0}^{x=1} \phi_n^2(x) dx$ . This equation provides a single relationship between two unknowns: mass and position. Thus, to determine the added mass, the beam must be actuated with the two first modes  $n = 1,2$  and the frequency shifts tracked for both. A 20-nanoresonator array was used to increase the detection cross-section. The resonance frequency of each resonator was tuned by varying its length. Resonators in the array ranged from 7.61  $\mu\text{m}$  to 10  $\mu\text{m}$  in length. They were 160 nm thick and 300 nm wide (**Figure S8**).

In previous work, the phenomena that influence mass measurements were listed. These include frequency noise and fabrication defects<sup>20</sup>. The influence of frequency noise is characterized, and a calibration method has been proposed to correct for fabrication defects. With the current design, the lower mass LOD was approximately 5 MDa, and the overall mass uncertainty was conservatively estimated to be within  $\pm 0.5$  MDa.

When frequency shifts are translated into the mass-position domain, a mass spectrum can be plotted. However, gold and silica nanoparticles were also characterized by average diameter and the standard deviation of their distribution. Thus, the mass distributions were converted into diameter distributions by computing the mass equivalent diameter for each particle, assuming the density of gold to be  $1.93 \times 10^4 \text{ kg/m}^3$ .

## Acknowledgments

The authors acknowledge support from the European Union through the ERC project Enlightened (Grant agreement # 616251), the LETI Carnot Institute NEMS-MS project, and the DGA Astrid NEMS-MS project. We thank M. Sansa for helpful discussions, and V. Brun for her feedback and support.

## Supporting Information Available:

Repeatability study data, Silica density characterization, NTP (NanoTetraPods) mass calculation, NMR-derived mass of grafted PEG on NTPs, NTP mass measured by ICP-MS, NEMS-MS architecture and NEMS particle sensor, information on aerodynamic focusing.

## Funding

This work was funded in part by the European Union through the ERC Enlightened project (GA #616251) and by CEA PTC Instrumentation/Detection (VIA-NEMS). In addition, K.L. thanks the National Natural Science Foundation of China (21975094) for financial support and the Jilin Province International Collaboration Base of Science and Technology (YDZJ202102CXJD004).

## Declaration on conflict of interest

C.M. and S.H. are co-inventors of patents US9506852B2, EP2779209A1, and JP6352004B2.

## References

- (1) Jeevanandam, J.; Barhoum, A.; Chan, Y. S.; Dufresne, A.; Danquah, M. K. Review on Nanoparticles and Nanostructured Materials: History, Sources, Toxicity and Regulations. *Beilstein J. Nanotechnol.* **2018**, *9* (1), 1050–1074. <https://doi.org/10.3762/bjnano.9.98>.
- (2) Zhu, Z. Gold Nanoparticle Based Biosensors. *New Dev. Gold Nanomater. Res.* **2016**, *43* (1), 95–116.
- (3) Kammers, A. D.; Daly, S. Self-Assembled Nanoparticle Surface Patterning for Improved Digital Image Correlation in a Scanning Electron Microscope. *Exp. Mech.* **2013**, *53* (8), 1333–1341. <https://doi.org/10.1007/s11340-013-9734-5>.
- (4) De Cicco, D.; Asaee, Z.; Taheri, F. Use of Nanoparticles for Enhancing the Interlaminar Properties of Fiber-Reinforced Composites and Adhesively Bonded Joints—a Review. *Nanomaterials* **2017**, *7* (11). <https://doi.org/10.3390/nano7110360>.
- (5) Cardoso, V. F.; Francesko, A.; Ribeiro, C.; Bañobre-López, M.; Martins, P.; Lanceros-Mendez, S. Advances in Magnetic Nanoparticles for Biomedical Applications. *Adv. Healthc. Mater.* **2018**, *7* (5). <https://doi.org/10.1002/adhm.201700845>.
- (6) Katz, L. M.; Dewan, K.; Bronaugh, R. L. Nanotechnology in Cosmetics. *Food Chem. Toxicol.* **2015**, *85*, 127–137. <https://doi.org/10.1016/j.fct.2015.06.020>.
- (7) Peters, R. J. B.; Bouwmeester, H.; Gottardo, S.; Amenta, V.; Arena, M.; Brandhoff, P.; Marvin, H. J. P.; Mech, A.; Moniz, F. B.; Pesudo, L. Q.; Rauscher, H.; Schoonjans, R.; Undas, A. K.; Vettori, M. V.; Weigel, S.; Aschberger, K. Nanomaterials for Products and Application in Agriculture, Feed and Food. *Trends Food Sci. Technol.* **2016**, *54*, 155–164. <https://doi.org/10.1016/j.tifs.2016.06.008>.
- (8) Jia, Y. P.; Ma, B. Y.; Wei, X. W.; Qian, Z. Y. The in Vitro and in Vivo Toxicity of Gold Nanoparticles. *Chinese Chem. Lett.* **2017**, *28* (4), 691–702. <https://doi.org/10.1016/j.ccllet.2017.01.021>.
- (9) Mahmoudi, M. The Need for Robust Characterization of Nanomaterials for Nanomedicine Applications. *Nat. Commun.* **2021**, *12* (1), 1–5. <https://doi.org/10.1038/s41467-021->

25584-6.

- (10) Carvalho, P. M.; Felício, M. R.; Santos, N. C.; Gonçalves, S.; Domingues, M. M. Application of Light Scattering Techniques to Nanoparticle Characterization and Development. *Front. Chem.* **2018**, *6* (June), 1–17. <https://doi.org/10.3389/fchem.2018.00237>.
- (11) Mourdikoudis, S.; Pallares, R. M.; Thanh, N. T. K. Characterization Techniques for Nanoparticles: Comparison and Complementarity upon Studying Nanoparticle Properties. *Nanoscale* **2018**, *10* (27), 12871–12934. <https://doi.org/10.1039/c8nr02278j>.
- (12) Holbrook, R. D.; Choquette, S. J. *NIST-Report of Investigation Reference Material 8011*; 2007.
- (13) Olesik, J. W.; Gray, P. J. Considerations for Measurement of Individual Nanoparticles or Microparticles by ICP-MS: Determination of the Number of Particles and the Analyte Mass in Each Particle. *J. Anal. At. Spectrom.* **2012**, *27* (7), 1143–1155. <https://doi.org/10.1039/c2ja30073g>.
- (14) Zhang, N.; Zhu, K.; Xiong, C.; Jiang, Y.; Chang, H. C.; Nie, Z. Mass Measurement of Single Intact Nanoparticles in a Cylindrical Ion Trap. *Anal. Chem.* **2016**, *88* (11), 5958–5962. <https://doi.org/10.1021/acs.analchem.6b00918>.
- (15) Keifer, D. Z.; Pierson, E. E.; Jarrold, M. F. Charge Detection Mass Spectrometry: Weighing Heavier Things. *Analyst* **2017**, *142* (10), 1654–1671. <https://doi.org/10.1039/c7an00277g>.
- (16) Scheffer, A.; Engelhard, C.; Sperling, M.; Buscher, W. ICP-MS as a New Tool for the Determination of Gold Nanoparticles in Bioanalytical Applications. *Anal. Bioanal. Chem.* **2008**, *390* (1), 249–252. <https://doi.org/10.1007/s00216-007-1576-5>.
- (17) Dominguez-Medina, S.; Fostner, S.; Defoort, M.; Sansa, M.; Stark, A. K.; Halim, M. A.; Vernhes, E.; Gely, M.; Jourdan, G.; Alava, T.; Boulanger, P.; Masselon, C.; Hentz, S. Neutral Mass Spectrometry of Virus Capsids above 100 Megadaltons with Nanomechanical Resonators. *Science* (80-. ). **2018**, *362* (6417), 918–922. <https://doi.org/10.1126/science.aat6457>.
- (18) Caputo, F.; Clogston, J.; Calzolari, L.; Rösslein, M.; Prina-Mello, A. Measuring Particle Size Distribution of Nanoparticle Enabled Medicinal Products, the Joint View of EUNCL and NCI-NCL. A Step by Step Approach Combining Orthogonal Measurements with Increasing Complexity. *J. Control. Release* **2019**, *299* (February), 31–43. <https://doi.org/10.1016/j.jconrel.2019.02.030>.
- (19) Dohn, S.; Svendsen, W.; Boisen, A.; Hansen, O. Mass and Position Determination of Attached Particles on Cantilever Based Mass Sensors. *Rev. Sci. Instrum.* **2007**, *78* (10), 1–4. <https://doi.org/10.1063/1.2804074>.
- (20) Clement, K.; Reynaud, A.; Defoort, M.; Vysotskyi, B.; Fortin, T.; Lai, S. H.; Çumaku, V.; Dominguez-Medina, S.; Hentz, S.; Masselon, C. Requirements and Attributes of Nano-Resonator Mass Spectrometry for the Analysis of Intact Viral Particles. *Anal. Bioanal. Chem.* **2021**, *413* (29), 7147–7156. <https://doi.org/10.1007/s00216-021-03511-4>.
- (21) Kim, W. W. K.; Kim, W. W. K.; Lee, K.; Son, M. J.; Kwak, M.; Chang, W. S.; Min, J. K.; Song, N. W.; Lee, J.; Bae, K. H. Corrigendum: A Reliable Approach for Assessing Size-Dependent Effects of Silica Nanoparticles on Cellular Internalization Behavior and Cytotoxic Mechanisms (Int J Nanomedicine. 2019; 14: 7375–7387.). *Int. J. Nanomedicine* **2020**, *15*, 10169–10170. <https://doi.org/10.2147/IJN.S295273>.

- (22) Tuoriniemi, J.; Johnsson, A. C. J. H.; Holmberg, J. P.; Gustafsson, S.; Gallego-Urrea, J. A.; Olsson, E.; Pettersson, J. B. C.; Hassellöv, M. Intermethod Comparison of the Particle Size Distributions of Colloidal Silica Nanoparticles. *Sci. Technol. Adv. Mater.* **2014**, *15* (3). <https://doi.org/10.1088/1468-6996/15/3/035009>.
- (23) Kimoto, S.; Dick, W. D.; Hunt, B.; Szymanski, W. W.; McMurry, P. H.; Roberts, D. L.; Pui, D. Y. H. Characterization of Nanosized Silica Size Standards. *Aerosol Sci. Technol.* **2017**, *51* (8), 936–945. <https://doi.org/10.1080/02786826.2017.1335388>.
- (24) Cheng, K.; Kothapalli, S. R.; Liu, H.; Koh, A. L.; Jokerst, J. V.; Jiang, H.; Yang, M.; Li, J.; Levi, J.; Wu, J. C.; Gambhir, S. S.; Cheng, Z. Construction and Validation of Nano Gold Tripods for Molecular Imaging of Living Subjects. *J. Am. Chem. Soc.* **2014**, *136* (9), 3560–3571. <https://doi.org/10.1021/ja412001e>.
- (25) Chang, Y. X.; Zhang, N. N.; Xing, Y. C.; Zhang, Q.; Oh, A.; Gao, H. M.; Zhu, Y.; Baik, H.; Kim, B.; Yang, Y.; Chang, W. S.; Sun, T.; Zhang, J.; Lu, Z. Y.; Lee, K.; Link, S.; Liu, K. Gold Nanotetrapods with Unique Topological Structure and Ultranarrow Plasmonic Band as Multifunctional Therapeutic Agents. *J. Phys. Chem. Lett.* **2019**, *10* (16), 4505–4510. <https://doi.org/10.1021/acs.jpcclett.9b01589>.
- (26) Lu, J.; Xue, Y.; Shi, R.; Kang, J.; Zhao, C. Y.; Zhang, N. N.; Wang, C. Y.; Lu, Z. Y.; Liu, K. A Non-Sacrificial Method for the Quantification of Poly(Ethylene Glycol) Grafting Density on Gold Nanoparticles for Applications in Nanomedicine. *Chem. Sci.* **2019**, *10* (7), 2067–2074. <https://doi.org/10.1039/C8SC02847H>.
- (27) Hartlen, K. D.; Athanasopoulos, A. P. T.; Kitaev, V. Facile Preparation of Highly Monodisperse Small Silica Spheres (15 to >200 Nm) Suitable for Colloidal Templating and Formation of Ordered Arrays. *Langmuir* **2008**, *24* (5), 1714–1720. <https://doi.org/10.1021/la7025285>.
- (28) Wang, X.; Kruis, F. E.; McMurry, P. H. Aerodynamic Focusing of Nanoparticles: I. Guidelines for Designing Aerodynamic Lenses for Nanoparticles. *Aerosol Sci. Technol.* **2005**, *39* (7), 611–623. <https://doi.org/10.1080/02786820500181901>.